

# A Novel Saliency Detection Method for Lunar Remote Sensing Images

Hui-Zhong Chen, Ning Jing, Jun Wang, Yong-Guang Chen, and Luo Chen

**Abstract**—The saliency detection provides an alternative methodology to semantic image understanding in many applications, for example, content-based image retrieval. To detect saliency for lunar remote sensing images, this letter proposes a crater feature model by analyzing the relationship between local interest points and saliency of lunar images. Based on the model, we propose a novel saliency detection method for lunar images. Our method merges and combines the speed-up robust feature features of the highlight region and shadow region of an impact crater to get the candidate regions of interest (ROI). Then, a descriptive feature vector is generated for each ROI, and the resulting saliency regions are distinguished from false detected and inconspicuous ones through a support vector machine. The method has been put into test on Chang'e-1 and Chang'e-2 lunar image data, and confirmed to be able to detect the salient region of impact craters correctly, with results much better than those obtained by the classical saliency detection method.

**Index Terms**—Lunar image, saliency detection, speed-up robust feature (SURF), support vector machine (SVM).

## I. INTRODUCTION

WITH the new round of lunar exploration recently, programs, such as the CLEMENTINE, LRO, SMART-1, SELENE, Chandrayaan-1, and Chang'e *et al.*, obtain a large quantity of lunar remote sensing data and make it available to the public soon after the mission. The large image databases are organized by keys such as mission Sol or spacecraft clock time, which makes it difficult to find concerned images and take advantage of the full potential of the data [1]. Content-based lunar image retrieval can find the relevant remote sensing lunar images from different data sources by considering the visual content, thereby greatly reducing the retrieval time.

The saliency refers to the visual attended parts in images and is confirmed effective for content-based image retrieval [2]. For lunar images, salient regions usually contain big and conspicuous impact craters. They are the most important visual contents according to human attention. Since lunar images are the lack of color information and the shapes of

Manuscript received February 26, 2012; revised June 16, 2012 and November 21, 2012; accepted November 21, 2012. Date of publication March 20, 2013; date of current version November 8, 2013. This work was supported in part by the National Natural Science Foundation of China under Grants 60902036, 61070035, and the National High Technology Research and Development Program of China under Grants 2008AA12A211, 2011AA120300. This paper was recommended by Associate Editor P. Gamba.

H.-Z. Chen is with the Department of Electronic Science and Engineering, National University of Defense Technology, Changsha 410073, China (e-mail: chen\_huizhong@yahoo.cn).

J. Jing and L. Chen are with the National University of Defense Technology, Changsha 410073, China (e-mail: ningjing@nudt.edu.cn; CL@nudt.edu.cn).

J. Wang is with the Third Research Institute of Ministry of Public Security, Shanghai 200031, China (e-mail: wangjun@nudt.edu.cn).

Y.-G. Chen is with the Ordnance Engineering College, Shijiazhuang 050003, China (e-mail: cyg@nudt.edu.cn).

Color versions of one or more of the figures in this paper are available online at <http://ieeexplore.ieee.org>.

Digital Object Identifier 10.1109/LGRS.2013.2244845

objects contained are about the same, they always appear to be very similar to each other and are difficult to distinguish, which improve the difficult of content-based lunar image retrieval. The detection of saliency is very helpful in reducing the impact of similar backgrounds and in making the extracted features more distinctive. So, it becomes an important research aspect of retrieving lunar images by their visual contents.

One of the most famous saliency detecting methods for images is Itti's model [3]. Other recent well-known works include [4]–[7]. These methods are designed for general images. They do not consider the specific visual features of lunar images, and therefore, the detection results are usually not satisfying. Besides these, there are methods called crater detection algorithms (CDAs) that are usually combinational methods using image processing and artificial intelligent techniques [8]–[11]. [12] summarized most existing CDAs, and [13] also considers highlight/shade regions to detect craters. However, aiming at geological uses (for example, counting the number of craters), CDAs do not consider the human attention, and the detection results may contain many insignificant small craters at the point of regions of interest (ROI) view.

The purpose of this letter is to introduce a novel saliency detection idea for lunar remote sensing images. Our approach differs from the existing works, in which we consider not only the human attention but also the specific features of lunar images. The approach is based on the interest points and statistical learning [14]. In our research, speed-up robust feature (SURF) [15] is used to get the highlight and shadow regions of lunar craters and combine them for the detection of the candidate ROI. After that, we generate a descriptive vector for each candidate ROI and then use a support vector machine (SVM) [16] to classification.

In the following sections, we describe a crater feature model and a saliency detection method based on the model in detail.

## II. CRATER FEATURE MODEL (CFM)

The salient region of the lunar remote sensing image usually consists of suspicious craters, which are the typical structures on the lunar surface. The appearances of craters in images are mainly determined by the sunlight and the shooting direction. Shown as Fig. 1, due to the angle between the sunlight and the lunar surface, only the part facing the sunlight is illuminated. Along the shooting direction, the illuminated part appears to be the highlight region of a crater in the image, and the back part appears to be the shadow region.

We use SURF to describe the highlight and shadow regions of lunar craters. SURF is a well-known performant interest point detector and descriptor, comprised of a feature detector based on Gaussian second derivative mask, and a feature descriptor that lies on Haar wavelet responses.

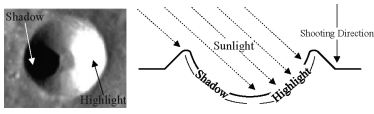


Fig. 1. Illumination of lunar impact crater. Left: the appearance of a typical crater contains a highlight region and a shadow region. Right: the corresponding illumination.

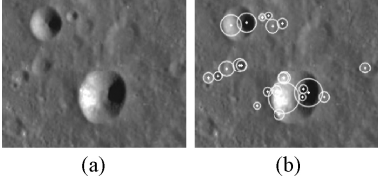


Fig. 2. SURF points of a lunar image. (a) Sample lunar remote sensing image with size 322×262 pixel. (b) Detected SURF points, the center of each circle denotes the position and the size denotes the scale.

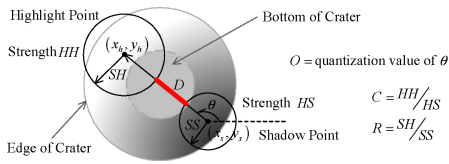


Fig. 3. Illustration of CFM: one pair of highlight and shadow points are used to construct the CFM, with elements including the orientation from highlight to shadow, the external distance, the strength contrast, and the scale ratio.

If a crater is visually salient, usually both of its highlight and shadow regions are outstanding in the image and SURF points can be detected. Here, we call the SURF points detected in highlight regions as highlight points and those in shadow regions as shadow points. Observed from Fig. 2, for a salient crater, at least one highlight point and one shadow point can be detected. While for inconspicuous ones, less or no point is detected. Therefore, the gathering areas of SURF points can describe the overview visual content of a lunar remote sensing image. The combination of nearby highlight and shadow points according to certain rules may figure out one salient crater. And, the set of these craters forms the saliency regions.

A crater feature model (CFM) is proposed based on the crater illumination feature and its relationship with SURF points. First define the highlight point as  $PH = (CH, SH, HH)$ . Here,  $CH = (x_h, y_h)$  corresponds to coordinate of its center,  $SH$  corresponds to the scale of the highlight point, and  $HH$  corresponds to the strength. Similarly, a shadow point is defined as  $PS = (CS, SS, HS)$ . Then, the CFM (Fig. 3) can be defined as  $CRATER = (PH, PS, O, D, C, R)$ .  $PH$  and  $PS$  of CFM refer to the highlight point and shadow point that construct the model. The other four elements are based on  $PH$  and  $PS$ , defined as follows.

$O$ : *Orientation*: The comparative direction of highlight and shadow. Let  $\theta$  be the angle between the line from the center of shadow point to the center of highlight point and the horizontal line, calculated according to the following equation:

$$\theta = \arctan((y_h - y_s) / (x_h - x_s)), \theta \in [0, 2\pi]. \quad (1)$$

Then, quantize  $\theta$  into eight parts in the range of  $[0, 2\pi]$  and correspondingly define  $O$  to eight values.

$D$ : *Distance*: The external distance of the highlight and shadow regions of a crater is calculated as

$$D = \begin{cases} 0, & \text{for } (y_h - y_s)^2 + (x_h - x_s)^2 \leq (SH + SS)^2 \\ ((y_h - y_s)^2 + (x_h - x_s)^2)^{\frac{1}{2}} - SH - SS, & \text{otherwise.} \end{cases} \quad (2)$$

$C$ : *Contrast*: The contrast of strength of the highlight and shadow points is calculated as

$$C = HH/HS. \quad (3)$$

$R$ : Ratio of the scale of the highlight point and the shadow point of a crater is calculated as

$$R = SH/SS. \quad (4)$$

Unlike CDAs, the purpose of saliency detection is distinguishing ROI of the lunar images, so CFM does not contain the illumination angle information and take no account of the diameter  $D$  of craters. As needed to distinguish highlight and shadow regions of crater, CFM is only suitable for lunar visible-light remote sensors images. And, the relative dimensions of the smallest structures, which CFM can detect, should be more than four pixels to differentiate the highlight and shadow regions.

### III. SALIENCY DETECTION METHOD

The saliency detection method for the lunar image is based on the CFM and has three main phases: preprocess, candidate regions of interest (ROI) detection, and classification.

#### A. Preprocess

In the preprocess phase, original lunar images are smoothed, contrast adjusted, and extracted the SURF points.

Original images of lunar surface from different data sources are usually of different contrast, sometimes being too bright or dark, and may contain unexpected noises. Thus, before extracting SURF features, we smooth the image and adjust the contrast automatically. Smoothing removes the small noises from the image. In our research, a Gaussian filter is applied to smooth an original lunar image and the following equation is used to adjust the contrast:

$$I'(x, y) = (I(x, y) - I_{min}) \times (2^b - 1) / (I_{max} - I_{min}). \quad (5)$$

The method for extracting SURF points is based on a fast-Hessian detector, as detailed in [15]. For each extracted feature, the sign of the Laplacian indicates that whether it is highlight or shadow, the location corresponds to the  $CH$  and  $CS$ , the scale corresponds to the  $SH$  and  $SS$  and the Hessian value indicates the  $HH$  and  $HS$ . In fact, we only concern about the detection. Therefore, it is unnecessary to calculate the high dimensional Haar-wavelet SURF descriptors.

#### B. Candidate ROI Detection

In the ROI detection phase, overlapping homogenous points are merged into one point and recalculated the center, scale and strength. After that, we combine the pairs of highlight and shadow points into ROI candidates by constructing the CFM according to several rules.

1) *Homogenous Feature Merge*: More than one SURF point may be detected within the same highlight or shadow region (see Fig. 2 for example). That is to say, detected homogenous points overlapped with each other are very likely to belong to the same highlight or shadow region. According to the definition of the CFM, we only consider one highlight point and one shadow point for each crater. To construct the model correctly and reduce the simplicity of the following calculation, overlapping homogenous points need to be merged.

The input of homogenous feature merge algorithm is the set of SURF points detected  $\{\text{PH}\} \cup \{\text{PS}\}$  as the result of preprocess phase. The main steps are as follows.

- 1) For the set of highlight points  $\{\text{PH}\}$ , sort in descending order of  $SH$ .
- 2) Let the first point in  $\{\text{PH}\}$  as  $\text{PH}_1$ .
- 3) For each  $\text{PH}_2 \in \{\text{PH}\}$  and  $\text{PH}_2 \neq \text{PH}_1$ , calculate the distance between  $CH_1 = (x_{h1}, y_{h1})$  and  $CH_2 = (x_{h2}, y_{h2})$

$$\text{Dist} = ((y_{h2} - y_{h1})^2 + (x_{h2} - x_{h1})^2)^{\frac{1}{2}}. \quad (6)$$

- 4) If the  $\text{Dist}$  is smaller than the scale  $SH_1$  of  $\text{PH}_1$  and no shadow point  $\text{PS}' \in \{\text{PS}\}$  that is near to  $\text{PH}_2$  (the distance between  $CH_2$  and  $CS'$  is smaller than a threshold defined as  $\text{Dist\_Threshold}$  that is defined as a statistics value of highlight shadow regions scale of sample images. In our paper,  $\text{Dist\_Threshold}$  equals 15 pixels. Generally, it is 1/20 to 1/30 of the image width) can be found, then  $\text{PH}_2$  can be merged with  $\text{PH}_1$ . In this condition, if  $\text{PH}_2$  is not in the region of  $\text{PH}_1$  ( $\text{Dist} + SH_2 > SH_1$ ), we merge  $\text{PH}_1$  and  $\text{PH}_2$  with their minimum bounding circle and calculate the new scale and new center position for  $\text{PH}_1$

$$SH_1 = \text{Dist} + SH_2 \quad (7)$$

$$\begin{cases} x_{h1} = x_{h2} + (x_{h1} - x_{h2}) \times \frac{(SH_1 - SH_2)}{\text{Dist}} \\ y_{h1} = y_{h2} + (y_{h1} - y_{h2}) \times \frac{(SH_1 - SH_2)}{\text{Dist}}. \end{cases} \quad (8)$$

Here, the  $SH_1$  in (8) is the newly calculated value by (7). When  $(\text{Dist} + SH_2 \leq SH_1)$ ,  $\text{PH}_1$  keeps the original value. If  $\text{PH}_1$  and  $\text{PH}_2$  are merged, remove  $\text{PH}_2$  from  $\{\text{PH}\}$ .

- 5) Let the next point in  $\{\text{PH}\}$  be  $\text{PH}_1$ . Repeat steps 3 and 4 for the remaining points.
- 6) For the set of shadow points  $\{\text{PS}\}$ , sort in descending order of  $SS$  and repeat steps 2 and 5 in a similar way as  $\{\text{PH}\}$ .
- 7) Return  $\{\text{PH}\} \cup \{\text{PS}\}$  as the set of merged feature points.

2) *ROI Combination*: The identification of ROI Candidates is achieved by combining highlight point with shadow one in pairs to construct the CFM. Considering the definition of the model, we propose the following constraints for combination.

*Constraint 1*: Orientation consistency. Define one main orientation  $O_{\text{main}}$  and two neighboring orientation  $O_{\text{left}}$ ,  $O_{\text{right}}$ . Only when the  $O$  of a pair of highlight and shadow point is equal to  $O_{\text{main}}$ ,  $O_{\text{left}}$  or  $O_{\text{right}}$ , can they be combined.

*Constraint 2*: Adjacency. Define a distance threshold  $D_{\text{max}}$ . The combination may occur when  $D \leq D_{\text{max}}$ .

*Constraint 3*: Strength restriction. Define an average value  $C_{\text{mean}}$ , an upper coefficient  $c_{\text{max}}$  and a lower coefficient  $c_{\text{min}}$ . When  $c_{\text{min}} \times C_{\text{mean}} \leq C \leq c_{\text{max}} \times C_{\text{mean}}$ , the combination is allowed.

*Constraint 4*: Scale restriction. Define an average value  $R_{\text{mean}}$ , an upper coefficient  $r_{\text{max}}$  and a lower coefficient

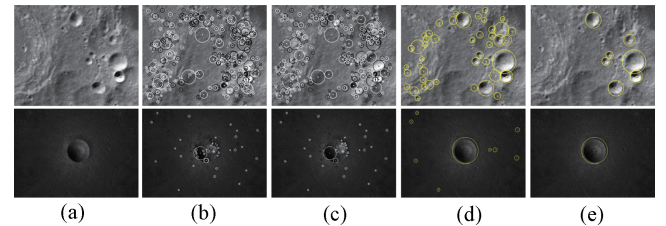


Fig. 4. Detection results for a Chang'e-1 (the first row, original image size  $217 \times 182$  pixel) and Chang'e-2 (the second row, original image size  $649 \times 453$  pixel) lunar remote sensing image. (a) Original images. (b) Extracted SURF feature points after preprocessing. The black circles denote the highlight points, and the white circles denote the shadow points. The point in each circle indicates the center position of feature point and the size of the circle be the scale. (c) Interest points after homogenous merge. (d) Detected candidate ROI. (e) Final saliency detection result.

$r_{\text{min}}$ . When  $r_{\text{min}} \times R_{\text{mean}} \leq R \leq r_{\text{max}} \times R_{\text{mean}}$ , the combination is allowed.

Based on the constraints, we propose a candidate ROI combination algorithm. The input of the algorithm is the set of merged feature points  $\{\text{PH}\} \cup \{\text{PS}\}$  and the output is ROI candidates, defined as  $\{\text{ROI}\} = \{(C_{\text{ROI}}, r, \text{CRATER})\}$ . It is a set of circular regions of radius  $r$  centering at  $C_{\text{ROI}} = (x_{\text{ROI}}, y_{\text{ROI}})$ , together with the corresponding crater feature model CRATER.

- 1) Sort  $\{\text{PH}\}$ ,  $\{\text{PS}\}$  in descending order of  $HH$  and  $HS$ . Let current pairs of highlight and shadow:  $\text{PH}_{\text{cur}}$  and  $\text{PS}_{\text{cur}}$  be the first points in  $\{\text{PH}\}$  and  $\{\text{PS}\}$ .
- 2) Check the constraints of current highlight and shadow pairs for constructing a CFM. If all the constraints are satisfied, go to step 3, else go to step 4.
- 3) Calculate the bias parameter

$$\text{bias} = \frac{|C_{\text{cur}} - C_{\text{mean}}|}{C_{\text{mean}}} \times \frac{|R_{\text{cur}} - R_{\text{mean}}|}{R_{\text{mean}}}. \quad (9)$$

And add  $\text{PS}_{\text{cur}}$  to the temporary set of the shadow candidates  $\{\text{PS}\}_{\text{temp}}$ .

- 4) Let the next point in  $\{\text{PS}\}$  be denoted as  $\text{PS}_{\text{cur}}$ . Repeat step 2 for the remaining points in  $\{\text{PS}\}$ .
- 5) If  $\{\text{PS}\}_{\text{temp}} \neq \emptyset$ , get the shadow candidate point with smallest  $\text{bias}$  from  $\{\text{PS}\}_{\text{temp}}$  as  $\text{PS}_{\text{cur}}$  and combine with  $\text{PH}_{\text{cur}}$  to construct a crater feature model CRATER. Calculate the corresponding ROI parameter

$$C_{\text{ROI}} : \begin{cases} x_{\text{ROI}} = (x_{\text{hcur}} + x_{\text{scur}})/2 \\ y_{\text{ROI}} = (y_{\text{hcur}} + y_{\text{scur}})/2 \end{cases} \quad (10)$$

$$r = SH_{\text{cur}} + SS_{\text{cur}} + D_{\text{cur}}/2. \quad (11)$$

Remove  $\text{PS}_{\text{cur}}$  from  $\{\text{PS}\}$  and add  $(C_{\text{ROI}}, r, \text{CRATER})$  into the resulting set of ROI:  $\{\text{ROI}\} = \{(C_{\text{ROI}}, r, \text{CRATER})\}$ .

- 6) Let  $\{\text{PS}\}_{\text{temp}} \leftarrow \emptyset$ . Let  $\text{PH}_{\text{cur}}$  be the next point in  $\{\text{PH}\}$  and  $\text{PS}_{\text{cur}}$  be the first point in  $\{\text{PS}\}$ . Repeat step 2 for the remaining points in  $\{\text{PH}\}$ .
- 7) Return  $\{\text{ROI}\}$  as the resulting candidate ROI.

### C. Classification

The supervised classification aims at removing the false detected and inconspicuous craters by SVM.

In addition to the craters, SURF points may be extracted in any salient region of the image, and these points are also likely to be falsely combined if they are not in conflict with the constraints. And, the neighboring orientation may aggravate the false detection. Moreover, the desired resulting saliency

regions should only contain salient craters; those noise-like small craters are not considered to be representative features of a lunar image. The supervised classification method is expected to remove both falsely combined craters and the inconspicuous small ones from the ROI results.

For the rules of classification, we consider the following.

- 1) Craters of large size are usually conspicuous.
- 2) Craters that are sharply contrast to the background are also likely to catch the observer's attention.
- 3) The neighboring orientation is one of the main reasons for the falsely combined.

Therefore, scale, strength, and orientation of a candidate ROI are used to form the feature vector for classification. Define  $f = \{f_1, f_2, f_3\}$  as the feature vector of a candidate ROI

$$f_1 = \frac{r}{r_{mean}} \quad (12)$$

$$f_2 = \frac{HH}{HH_{mean}} \times \frac{HS}{HS_{mean}} \quad (13)$$

$$f_3 = \begin{cases} 1, & \text{for } O = O_{main} \\ 1 - (|\theta - \frac{\pi}{4} \times (O_{main} - 1)| - \frac{\pi}{8}) / \frac{\pi}{4}, & \text{otherwise.} \end{cases} \quad (14)$$

$f_1$  is the ratio of the size  $r$  to  $r_{mean}$ , and  $r_{mean}$  is the mean size value of all the ROI in the same image.  $f_2$  is the ratio of strength of the ROI to the average highlight strength and average shadow strength.  $f_3$  denotes the deflective angle. If the orientation of the candidate ROI is equal to the main orientation of the image,  $f_3$  is set to 1. Or, else, when it is the neighboring orientation, a deflective angle will be calculated according to (14). All three elements take the corresponding mean value into consideration so as to make better description when the lunar images are of different types.

After calculating the feature vector for each ROI candidate, an SVM is applied for classification, which identifies the false combined or inconspicuous ROI and leave salient crater regions as the output results. Here, we use the standard C-SVM with a radial-base function as the kernel function. Before the classification, a training sample is used to generate the model and the necessary parameters.

#### IV. EXPERIMENTAL RESULTS

We tested the proposed saliency detection method on the Chang'e-1 and Chang'e-2 lunar image data,<sup>1</sup> which resolutions are 120 m and 7 m separately, and compared the detection results with that by Itti's model [3]. Some CLEMENTINE data,<sup>2</sup> which resolution is 100 m, is also used for comparison. The program of our saliency detection method was developed with Microsoft Visual C++ 2008 and OpenCV 2.0. The results by Itti's model were generated using MATLAB 7.4 and SaliencyToolbox 2.1.<sup>3</sup>

Fig. 4 shows the detection results by our method of a Chang'e lunar images. The illustrations of each step and the final saliency detection results are given. Observed from the figures, SURF features after preprocessing gather at the regions where the surface is of complex structure, which distinguishes the potential attended regions from the plane background [see Fig. 4(b)]. Fig. 4(c) shows that after homogeneous merge the numbers of feature points are reduced, many overlapped small points in Fig. 4(b) disappear in Fig. 4(c) by merging with larger ones. The detected candidate ROI in Fig.

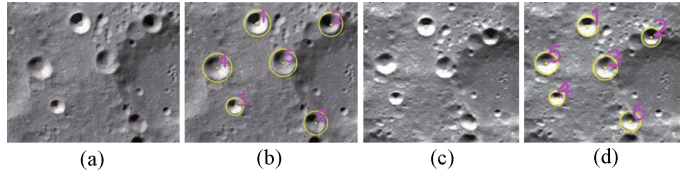


Fig. 5. Detection results from different datasources. (a) Original Chang'e-1 lunar image with size 277×225 pixel. (b) Detection result of (a). (c) Original CLEMENTINE lunar image of the same area with size 181×163 pixel. (d) Detection result of (c). The numbers indicate the saliency ranked during the classification phase.

TABLE I  
STATISTIC ANALYSIS INFORMATION ABOUT  
THE EXPERIMENTAL DATASETS

(11073 Craters Labeled)	Best	Worst	Average
Detected salient craters	100%	66.67%	92.18%
Detected less salient craters	0%	27.27%	8.75%
Detected unsalient craters	0%	0%	0%
Falsely detected	0%	15.38%	2.37%

4(d) includes the saliency regions together with the areas of craters together with many false detected and inconspicuous ones. For Chang'e-1 data, in regions where the backgrounds are complex, many false craters are detected. However, after supervised classification [see Fig. 4(e)] the less salient and falsely detected crater candidates are removed. Referring to the original images Fig. 4(a), it can be found that our method is able to detect the saliency regions of lunar image precisely. The results only contain those salient craters and ignore the inconspicuous and false ones, which is similar to human attention. Therefore, our saliency detection result can be a summary of the visual content of a lunar image.

Fig. 5 gives out the saliency detection results by our method upon images of the same area from two different datasources (Chang'e-1 and CLEMENTINE). Observed from the figure, the two original images do not appear to be very similar, because the sunlight direction and the gray-scale contrast are quite different. For both images, our method works well in the detection of the main crater regions. The saliency ranking order of the corresponding saliency regions may not be the same due to their different appearance, for example, the crater region 5 detected in Chang'e-1 image [see Fig. 5(b)] is ranked as 3 in Fig. 5(d) because it looks much brighter in the CLEMENTINE image. However, it has little influence because the two results [see Fig. 5(b) and (d)] are about the same that both of them contain the same six main crater regions. It proves that the detection results by our method can represent the main visual content for images from different datasources and can establish the relationship between images of same areas.

Fig. 6 presents comparisons with our method against the Itti's model. Three lunar images are detected for comparison. As shown in the figure, the Itti's model usually cannot detect the whole salient crater, which usually contain part of backgrounds or split one crater. And for the right three images that is partial of Sinus Iridum, Itti's model fails to detect the two upper salient craters. In contrast, the results of our method fit the edge of craters very well and contain few backgrounds. The main reason is that CFM has considered the human knowledge about craters and lunar images for the specific features of lunar images.

To test effectiveness of our method, we labeled 11073 ROIs of 1190 lunar images from Chang'e (736 images) and CLEMENTINE (454 images) manually, Fig. 7 is an example

<sup>1</sup>Available at <http://moon.bao.ac.cn>.

<sup>2</sup>Available at <http://nssdc.gsfc.nasa.gov/planetary/clementine.html>.

<sup>3</sup>Available at <http://www.saliencytoolbox.net>.

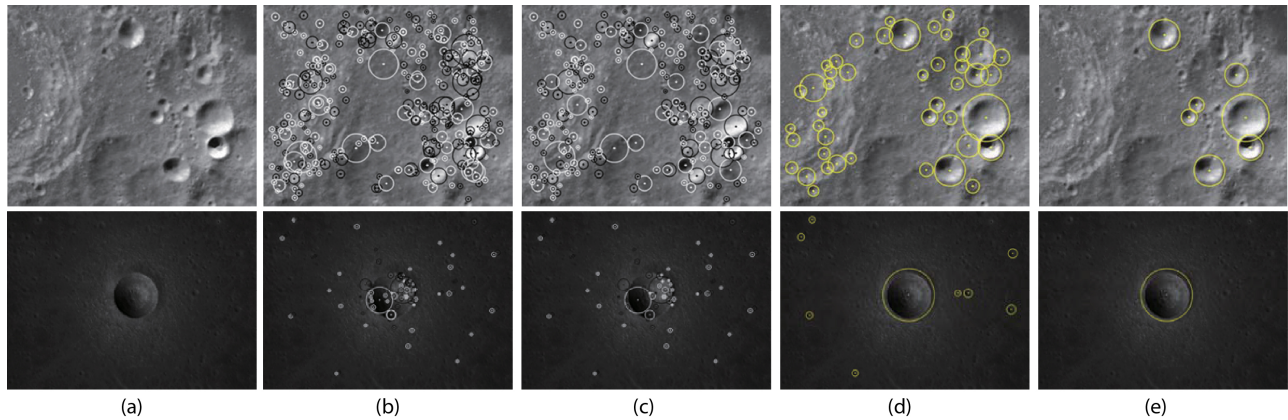


Fig. 6. Detection results compared with Itti's model. (a) Original images. (b) Saliency detected by Itti's model. (c) Our results. ((d)-(f) Partial images of Sinus Iridum, size 469×730 pixel.

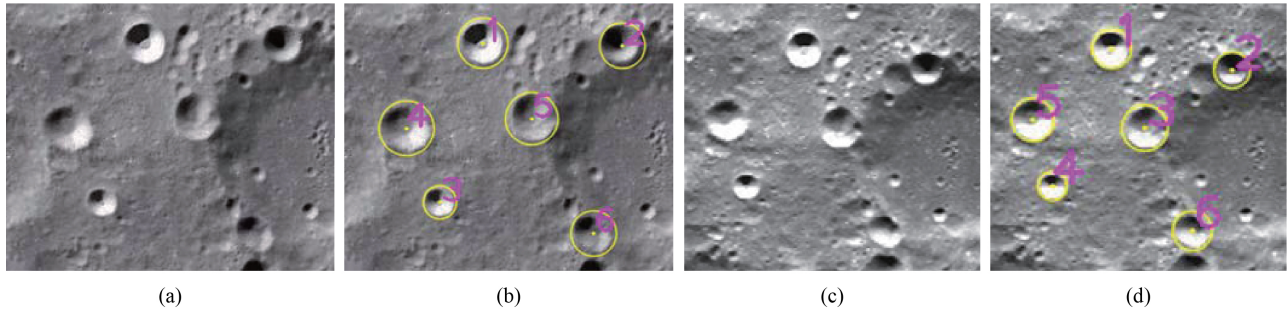


Fig. 7. Example of manual labeling.

of ROI detection by humans. The left figure is an original image, the red regions on the right figure denote the most salient ROI of the original image, and the blue regions denote the less salient ROI. We also have statistics results of our method on these images, and Table I presents the detailed information. The value is proportion of regions detected by our method in the regions labeled by humans. From statistics results, the average of detection is 92.18%, which is a high ROI detection ratio.

## V. CONCLUSION

In this letter, a method was proposed for detecting the saliency regions in lunar remote sensing images. Unlike existing saliency detection methods or CDAs, our methods took both human attention and specific visual features of lunar images into account. The method was simply designed and described in detail. It was based on SURF interest points to generate candidate ROI that may contain the salient craters. Furthermore, an SVM is used for supervised classification to detect the final saliency results. Experiments and comparison upon the real lunar images show that our method had a good detection effect—precise and in accordance with human attention.

The appearance of lunar images may be different for many reasons, such as sun elevation and azimuth. In some cases, the highlight and shadow regions are not obvious. For better solutions, our future work will consider other feature descriptors and combine them with the method in this letter.

## REFERENCES

- [1] C. Meyer and M. Deans, "Content based retrieval of images for planetary exploration," in *Proc. IEEE/RSJ Int. Conf. Intell. Robots Syst.*, 2007, pp. 1377–1382.
- [2] K. Vu, K. Hua, and W. Tavanapong, "Image retrieval based on regions of interest," *IEEE Trans. Knowledge Data Eng.*, vol. 15, no. 4, pp. 1045–1049, Jul.–Aug. 2003.
- [3] L. Itti, C. Koch, and E. Niebur, "A model of saliency-based visual attention for rapid scene analysis," *IEEE Trans. Pattern Anal. Mach. Intell.*, vol. 20, no. 11, pp. 1254–1259, Nov. 1998.
- [4] R. Achanta, S. Hemami, F. Estrada, and S. Sussman, "Frequency-tuned salient region detection," in *Proc. IEEE Conf. Comput. Vision Pattern Recognit.*, Jun. 2009, pp. 1597–1604.
- [5] T. Liu, Z.-J. Yuan, J. Sun, N.-N. Zheng, X. Tang, and H.-Y. Shum, "Learning to detect a salient object," *IEEE Trans. Pattern Anal. Mach. Intell.*, vol. 33, no. 2, pp. 353–367, Feb. 2011.
- [6] J. Harel, C. Koch, and P. Perona, "Graph-based visual saliency," in *Proc. Adv. NIPS*, vol. 19, 2007, pp. 545–552.
- [7] X. Hou and L. Zhang, "Saliency detection: A spectral residual approach," in *Proc. IEEE Conf. Comput. Vision Pattern Recognit.*, Jun. 2007, pp. 1–8.
- [8] D. Bue and F. Stepinski, "Machine detection of martian impact craters from digital topography data," *IEEE Trans. Geosci. Remote Sensing*, vol. 45, no. 1, pp. 265–274, Jan. 2007.
- [9] L. Bandeira, J. Saraiva, and P. Pina, "Impact crater recognition on mars based on a probability volume created by template matching," *IEEE Trans. Geosci. Remote Sensing*, vol. 45, no. 12, pp. 4008–4015, Dec. 2007.
- [10] R. Martins, P. Pina, J.-S. Marques, and M. Silveira, "Crater detection by a boosting approach," *IEEE Geosci. Remote Sensing Lett.*, vol. 6, no. 1, pp. 127–131, Jan. 2009.
- [11] G. Troglio, J. Le Moigne, J.-A. Benediktsson, G. Moser, and S.-B. Serpico, "Automatic extraction of ellipsoidal features for planetary image registration," *IEEE Geosci. Remote Sensing Lett.*, vol. 9, no. 1, pp. 95–99, Jan. 2012.
- [12] G. Salamunicar, S. Loncaric, P. Pina, L. Bandeira, and J. Saraiva, "Mai 30301gt catalogue of martian impact craters and advanced evaluation of crater detection algorithms using diverse topography and image datasets," *Planetary Space Sci.*, vol. 59, no. 1, pp. 111–131, 2011.
- [13] R. Urbach, and F. Stepinski, "Automatic detection of sub-km craters in high resolution planetary images," *Planetary Space Sci.*, vol. 57, no. 7, pp. 880–887, 2009.
- [14] V. N. Vapnik, *The Nature of Statistical Learning Theory*. New York, USA: Springer-Verlag, 1995.
- [15] S. Bay, T. Tuytelaars, and L. Gool, "Surf: Speeded up robust features," in *Proc. Eur. Conf. Comput. Vision*, 2006, pp. 404–417.
- [16] C. Cortes and V. Vapnik, "Support-vector networks," *Mach. Learning*, vol. 20, no. 6, pp. 273–297, 1995.